Chitosan-transition metal coordination biopolymer: A promising heterogeneous catalyst for radical ion polymerization of vinyl acetate at ambient temperature.

Ibraheem Olayiwola Bisiriyu and Reinout Meijboom

Department of Chemical Sciences, University of Johannesburg, PO Box 524, Auckland Park, Johannesburg 2006, South Africa.

Email: rmeijboom@uj.ac.za, bisiriyy@yahoo.com

**Author for correspondence email: rmeijboom@uj.ac.za, Tel: +27115592367*

Abstract

The present study utilized chitosan obtained from crab shell and transition metal salts as precursors to synthesize chitosan-metal coordination biopolymers of Mn(II), Fe(III), Co(II) and Ni(II) [i.e Chit-Mn(II), Chit-Fe(III), Chit-Co(II) and Chit-NI(II) respectively]. The synthesized coordination biopolymers have been characterized using different instrumental techniques such as spectroscopic (UV-visible, FT-IR, XRD, EDS, and ICP-OES), thermal analysis (TGA and DTA), surface analysis (SEM), and hydrogen-temperature programmed reduction (H_2-TPR) analysis. Spectroscopic studies confirmed the successful incorporation of the metals into the biopolymer matrix. Thermal analysis and H_2-TPR revealed the reducibility of the Chit-Fe(III) at 120 ℃. While Chit-Fe(III) and Chit-Ni(II) were inactive, Chit-Co(II) and Chit-Mn(II) were found to be active towards vinyl acetate polymerization in the presence of aqueous Na_2SO_3. Furthermore, the polyvinyl acetate (PVAc) produced from Chit-Co(II) compared perfectly with a commercial PVAc and was in higher yield than PVAc produced from Chit-Mn(II). The polymerization has been shown to proceed via surface-initiated atom transfer radical polymerization (SI-ATRP), and the viscosity average molecular weight of PVAc produced has been measured as 25, 078. The density functional theory approach has been used to ascertain the coordination orientation of the Chit-Co(II) and explain its high efficiency towards vinyl acetate polymerization. The catalyst reusability test revealed an insignificant loss of activity for the Chit-Co(II) after seven cycles of polymerization. Kinetic studies show that the vinyl acetate polymerization suits the second-order kinetic model at ambient temperature. Thermodynamic studies also revealed that chain initiation is an endothermic process while chain propagation is an exothermic process. The result of this work also suggests an investigation of chitosan-metal coordination biopolymer via low-ppm ATRP approach for possible biomedical application.

Keywords: Chitosan-metal coordination biopolymer; polyvinyl acetate; viscosity average molecular weight; Density functional theory; Surface-initiated atom transfer radical polymerization.

1.0. Introduction

Polyvinyl acetate is one of the vinyl polymers which are known to make up the largest family of synthetic polymers with numerous applications. Thus, it is desirable to investigate the catalysis of vinyl acetate polymerization from the perspective of cost viability and green chemistry. Recently, homogeneous catalyst systems are gradually being replaced by heterogeneous ones as an advancement in chemical synthesis. Heterogeneous catalysis systems are known to provide advantages which include the ease with which catalyst can be removed, recovered, and recycled [1] [2]. Chitosan (fig. S1 Supplementary Information) has been reported to be a cheap and green renewable material [1] [3] [4] [5] [6] [7] [8]. Additionally, it is clear that chitosan could be utilized as an effective, reusable, and eco-friendly catalyst support in different applications [9]. Moreover, there has been a rise in the use of chitosan as a novel material for catalyst support in heterogeneous catalysis due to its high affinity towards metal ions [1] [10]. Even though the initiation of vinyl polymerization by Chitosan-Cu(II) biopolymer complex was found by Yoshiaki and co-workers in 1978 [11], the foremost disclosure of living radical polymerization was credited to Otsu and collaborators in 1982 [12]. Following Otsu's discovery was the rise of different living radical polymerization methods [13] of which reversible addition-fragmentation chain transfer radical polymerization (RAFT), nitroxide-mediated polymerization (NMP), and atom transfer radical polymerization (ATRP) have been adjudged as the three most popular controlled living radical polymerization (C/LRP) (or reversible-deactivation radical polymerization, RDRP) techniques [14]. While NMP and RAFT suffer the set-back of higher reaction temperature and multi-step reactions for chain transfer generation, respectively, transition metal-mediated (particularly, copper-mediated) atom transfer radical polymerization (ATRP) remains the commonly used technique owing to simpler reaction condition, ATRP initiators, and ligands availability [13]. In the same vein, several ATRP methods have been created to improve the polymerization process which includes, normal ATRP [15] [16] [17] [18] [19], reverse ATRP [20], simultaneous reverse and normally initiated (SR&NI) ATRP [21] [22], activators generated by electron transfer (AGET) ATRP [23] [24] [25], activators regenerated by electron transfer (ARGET) ATRP [26] [27] [28],

initiators for continuous activator regeneration (ICAR) ATRP [29] [30], supplemental activators and reducing agents (SARA) ATRP [31] [32] [33], single-electron transfer-degenerative transfer living radical polymerization (SET-DTLRP) [34] and single-electron transfer living radical polymerization (SET-LRP) [35] [36] [37] [38] [39] [40]. All of these systems require an ATRP initiator and an activator (usually metal complex in the lower oxidation state mostly generated by the addition of a reducing agent) before the polymerization of a vinyl monomer can proceed. Most of the reported works on chitosan based biopolymer in ATRP and other RDRP techniques are done to load initiators on chitosan or to modify chitosan for application in other fields like pharmaceuticals, water treatment, biomedicine, etc. [41][42]. However, with the use of a chitosan-metal coordination biopolymer, only a reducing agent is needed for the vinyl monomer polymerization to proceed, but the mechanism of polymerization has not been fully studied. Since the discovery of Yoshiaki and associates [11], little effort has been committed towards the investigation of the impact of the metal on catalyst performance. Most chitosan-metal complexes have been used in hydrogenation [43], hydration [1], adsorption [44] [45], cross-coupling reaction [46], cycloaddition reaction [10] [7] and photocatalysis [47] [48]. To date, the detailed reports on the use of chitosan-metal catalysts for vinyl acetate polymerization are limited. Chitosan-Co(II) [49] [50] and chitosan-Zn(II) [51] have recently been investigated for vinyl acetate polymerization. However, cobalt has been found to be more effective than zinc [49] [50] [51]. Due to the high cost of the second row, third row, and the late transition elements, this study has been geared towards the effect of some first-row transition metals (Ni, Mn, Co, and Fe) on vinyl acetate polymerization with insight into the possible reaction mechanism. Though, various studies have shown that the performance and activity of metal complexes when used as catalyst strongly depend on the structure of the ligand as well as to the electronic properties of the center metal [52]; the chemical modification of the structure of chitosan before complexation can be dedicated to further studies. In order to investigate the effect of the selected first-row transition metals for vinyl acetate polymerization, a series of chitosan-metal complexes were prepared with different metals and were characterized using Uv-visible spectroscopy, Fourier transforms infrared (FT-IR) spectroscopy, X-ray diffraction (XRD) spectroscopy, inductively coupled plasma optical emission spectroscopy (ICP-OES), hydrogen-temperature-programmed reduction (H_2-TPR), thermal analysis and scanning electron microscopy-energy dispersive spectroscopy (SEM-EDS). Reaction optimization, rate of vinyl acetate polymerization, and the thermodynamic parameters were studied by

polymerizing a few milliliters of the monomer in a small poly-top vial as a one-pot system. The experimental details and results are thus presented.

2.0. Experimental

2.1. Materials and Instrumentations

All analytical grade chemicals were used without additional purification and were obtained from Sigma-Aldrich. Reagent-grade chemicals were used with distilled water to prepare all aqueous solutions. Standard Schlenk systems under nitrogen atmosphere were used where experiments involving air as well as moisture-sensitive compounds were performed. $CoCl_2 \cdot 6H_2O$, $MnCl_2 \cdot 4H_2O$, $NiCl_2$, and $Fe(NO_3)_3 \cdot 9H_2O$ were used as the metallic precursor. The deacetylation degree for chitosan was determined to be 96% by the NMR spectroscopic method [53] [54] [55]. UV-visible spectra were obtained with a Shimadzu UV-1800 spectrophotometer. Fourier transform infrared (FT-IR) spectra were acquired with a Shimadzu IRAffinity-1S. Thermal analysis was determined using METTLER TOLEDO DSC822^e and SDTQ600 thermogravimetric analyzer (TA instrument). The percentage of metal loadings of the complexes were determined using inductively coupled plasma optical emission spectroscopy (ICP-OES). The hydrogen-temperature-programmed reduction was studied using the Micromeritics Autochem II chemisorption analyzer. X-ray diffraction (XRD) patterns were analyzed using a Rigaku Miniflex 600 diffractometer. The surface morphology of the samples was confirmed using Tescan Vega 3 LMH Scanning electron microscopy (SEM). The polymerization of vinyl acetate was carried out as previously reported [48] [49] [50]. The vinyl polymer obtained was analyzed using Bruker Avance III HD (500 MHz equipped with Bbi probe) NMR spectrometer with the same FT-IR spectrometer and UV-visible spectrometer used to characterize the coordination biopolymer. The viscosity average molecular weight of the polymer was obtained from the Mark-Houwink equation by first determining the intrinsic viscosity using the 1835 parallel Ubbelohde viscometer.

2.2. Synthetic procedures

2.2.1. Synthesis of chitosan-Co (Chit-Co(II)), chitosan-Ni (Chit-Ni(II) and chitosan-Mn (Chit-Mn(II))

1 g of chitosan (Chit) was dispersed in 25 ml of the metal ions solution containing 10 wt% of metal with respect to the chitosan biopolymer. The mixture was stirred vigorously with a magnetic stirrer under an inert atmosphere for 24 h to afford the formation of the biopolymer metal complexes (Scheme 1a). The suspensions were filtrated, and the coordination polymers were washed repeatedly with acetone; then dried at 60 ºC in a vacuum oven for 24 h.

2.2.2. Synthesis of chitosan-Fe (Chit-Fe(III))

1 g of chitosan (Chit) was added to a 25 ml solution of $Fe(NO_3)_3 \cdot 9H_2O$ containing 10 wt% of Fe with respect to the chitosan biopolymer. The mixture was stirred vigorously with a magnetic stirrer under an inert atmosphere for 24 h (Scheme 1b). The resulting brown gelly-like solution was transferred into a petri-dish and allowed to dry. A biopolymer film (chitosan-Fe(III)) was obtained after 24 h.

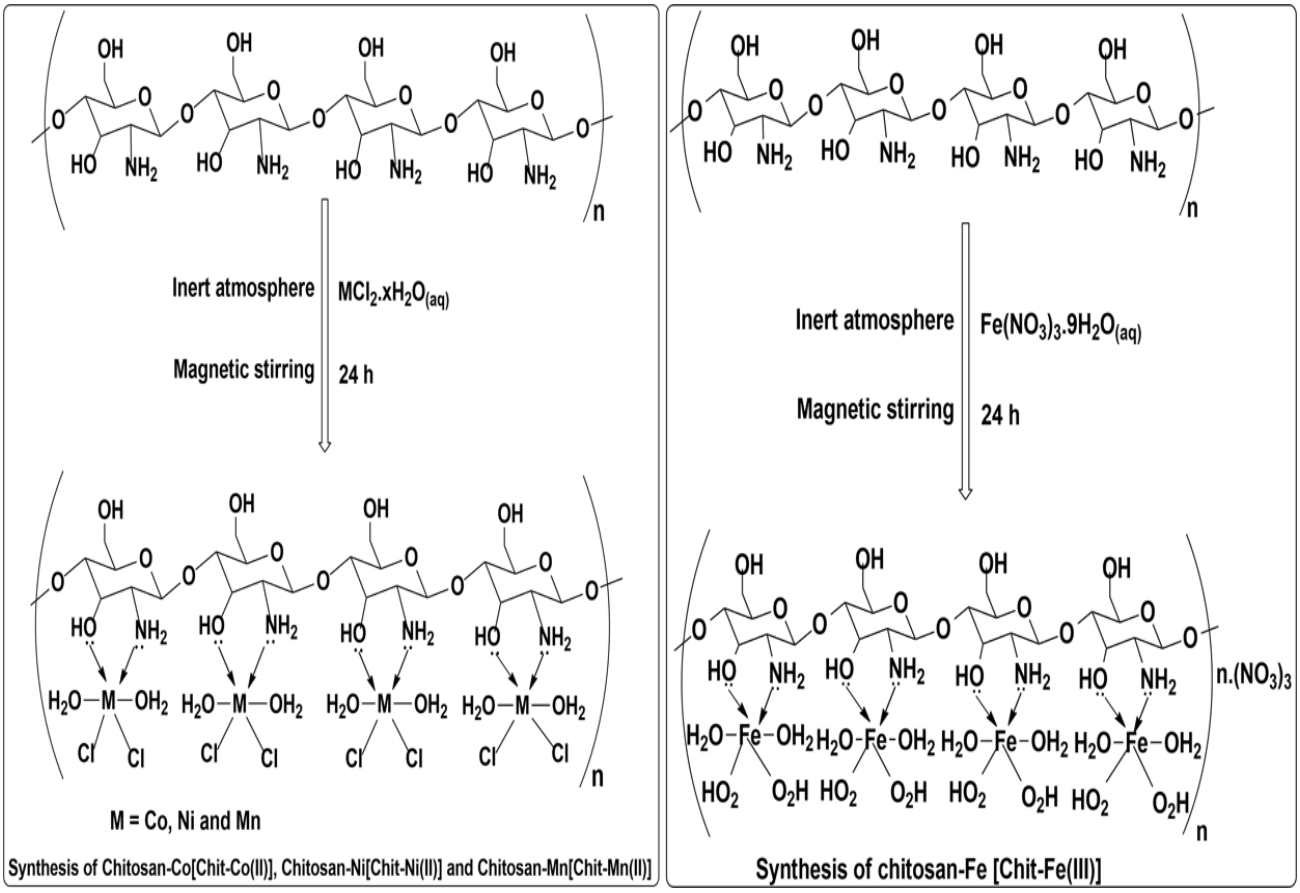

Scheme 1: (a) Synthesis of Chitosan-Co(II), Chitosan-Ni(II) and Chitosan-Mn(II) Coordination biopolymers (b) Synthesis of Chitosan-Fe(III) Coordination biopolymer

2.2.3. Computational studies

Interestingly, the coordination orientation of the synthesized chitosan-metal coordination biopolymers [namely Chit-Co(II), Chit-Ni(II), and Chit-Mn(II)] cannot easily be ascertained due to various possible coordination modes. Therefore, four different isomers were proposed for each coordination polymer base on a coordination number of six and using a unit of the coordination complex. The stability of these isomers was examined by computational technique. The isomers were first pre-optimized with Avogadro; then geometry optimization was carried out with ORCA using RI-PBE/def2-SVP level of theory, and the final single point energy for each isomer was recorded [56] [57] [58] [59]. Geometry optimization was also carried out for the Chitosan monomer unit (Chit-unit) and the Chit-Fe(III) unit complex using the same method. The HOMO and LUMO orbitals of Chit-unit, Chit-Fe(III), as well as the most stable isomer of Chit-Co(II), Chit-Ni(II), and Chit-Mn(II) were visualized with MOLDEN, and the HOMO – LUMO energy gaps were calculated.

2.3. Polymerization of vinyl acetate

Using the coordination biopolymers [Chit-Co(II), Chit-Ni(II), Chit-Mn(II), and Chit-Fe(III)] prepared as catalysts, vinyl acetate polymerization was carried out using the previous method [50] [51]. In a typical experiment, 0.01 g of the catalysts were added separately into a vial containing a biphasic mixture of 1 ml vinyl acetate monomer and 1 ml Na_2SO_3 aqueous solution (figure 1). The catalyst settles at the junction between the aqueous and organic layers. After allowing the mixture to stand for a while, a white precipitate begins to appear at the catalyst surface and grows into the aqueous phase. The polymer obtained (PVAc) after 24 h was filtered, washed with distilled water, and finally dried at 80 ºC in an oven. The percentage yield was calculated using GC-FID base on the decrease in the amount of the vinyl acetate monomer by taking a small portion of the organic phase using decane as the internal standard. The PVAc was characterized using Infrared spectroscopy, UV-visible spectroscopy, NMR spectroscopy, and SEM-EDS. The viscosity average molecular weight of the PVAc was obtained from the Mark-Houwink equation 1.

$$[\eta] = KM^{\alpha} \quad (1)$$

Where [η] is the intrinsic viscosity, M molecular weight, K, and α are constants for a particular polymer-solvent system (in this case, polyvinyl acetate-acetone system). To measure the intrinsic viscosity, solutions of PVAc in acetone were prepared with varying concentrations; the time of flow of the solvent (t_0) and solutions (t) between the upper and lower mark of the viscometer were measured and were used to determine the polymer relative viscosity (η_r), specific viscosity (η_{sp}), reduced viscosity (η_{red}) and inherent viscosity (η_{Inh}) according to equations 2, 3, 4 and 5 respectively.

$$\eta_r = \frac{t}{t_0} \tag{2}$$

$$\eta_{sp} = \frac{t - t_0}{t_0} = \eta_r - 1 \tag{3}$$

$$\eta_{red} = \frac{\eta_{sp}}{C} \tag{4}$$

$$\eta_{Inh} = \frac{\eta_r}{C} \tag{5}$$

Where C is the concentration of the polymer solution, the intrinsic viscosity [η] was obtained from the reduced and inherent viscosity in accordance with equation 6. The calculated reduced viscosities and inherent viscosities were plotted against the individual polymer concentration. The two graphs were extrapolated to obtain a common ordinate designated as intrinsic viscosity [η].

$$[\eta] = \left(\frac{\eta_{sp}}{C}\right)_{C\to 0} = \left(\frac{\eta_r}{C}\right)_{C\to 0} \tag{6}$$

2.4. Optimization of reaction conditions

The best catalyst from the polymerization study was used at ambient temperature for the optimization of the reaction conditions viz: Catalyst-monomer ratio, reducing agent (Na_2SO_3) concentration, monomer-reducing agent ratio, and monomer-reducing agent contact area.

2.4.1. Catalyst-Monomer ratio (CM ratio)

The effect of the catalyst-monomer ratio on the yield of polymerization was studied by adding various masses of catalyst (in gram) into the biphasic mixture of vinyl acetate monomer (1 ml) and $Na_2SO_{3(aq)}$ (1ml) at 25 °C. After 24 h of standing, the percentage yield of PVAc in each case was determined and plotted against the respective catalyst amount per 1 ml of monomer liquid.

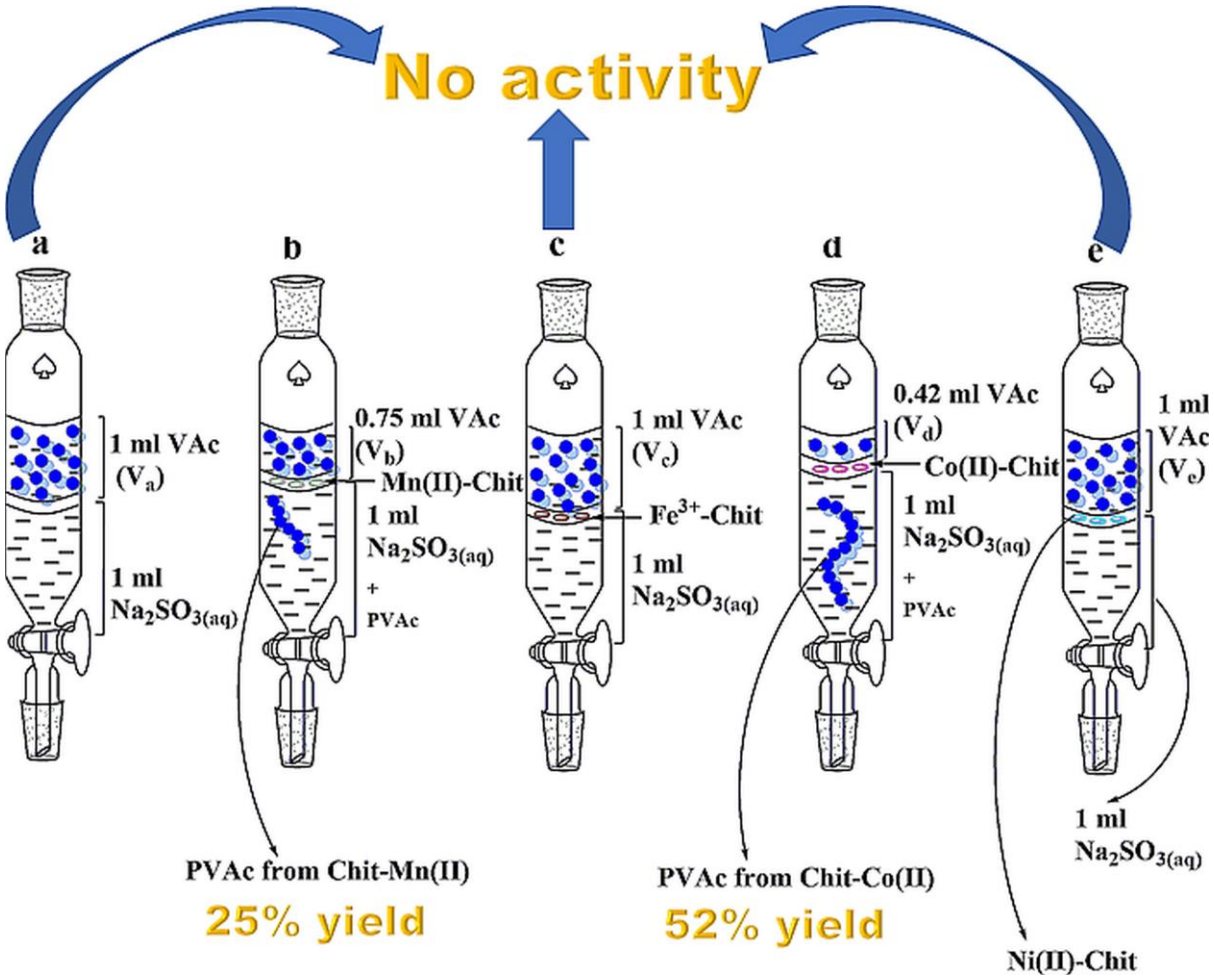

[Na_2SO_3] = 1M, VAc:Na_2SO_3 = 1vol/1vol, Chit-M:VAc = 0.01g/ml, MR area/MV = 1.3893 cm^{-1}

Figure 1: Polymerization of vinyl acetate in sodium sulphite solution for 24 h at 25 °C using (a) no catalyst (b) Chit-Mn(II) as catalyst (c) Chit-Fe(III) as catalyst (d) Chit-Co(II) as catalyst (e) Chit-Ni(II) as catalyst

2.4.2. Reducing agent concentration (RC)

The effect of Na_2SO_3(aq) concentration on the yield of polymerization of vinyl acetate was investigated by preparing a series of Na_2SO_3(aq) with concentrations ranging from 0.2 to 2.0 M. Optimum mass of catalyst per 1 ml of the monomer was added into the prepared Na_2SO_3(aq)

solutions and allowing polymerization to take place for 24 h at 25 ℃. The percentage yields obtained were plotted against Na_2SO_3(aq) concentrations.

2.4.3. Monomer-Reducing agent ratio (MR ratio)

After identifying the optimum reducing agent concentration, the effect of the monomer-reducing agent ratio was investigated by keeping the catalyst-monomer ratio constant and polymerizing with varied Na_2SO_3(aq) amount at 25 ℃ for 24 h. The percentage yield in each case was calculated and plotted against the monomer-reducing agent ratio.

2.4.4. Monomer-Reducing agent contact area (MR area) to Monomer Volume (MV) ratio

Stirring the reaction mixture will typically increase the MR area to MV ratio. As the stirring rate is increased, the MR area to MV ratio is expected to increase. However, it appears that stirring disfavoured the polymerization process, probably due to chain termination by rapid bimolecular combination and chain disproportionation. Conversely, by keeping other conditions constant, the effect of the monomer-reducing agent contact area was examined by polymerizing vinyl acetate in different vials with a different internal cross-sectional area at 25 ℃ for 24 h. The percentage yield in each case was calculated and plotted against the MR area to MV ratio.

2.5. Kinetics and thermodynamic studies of vinyl acetate polymerization

For kinetic measurement, the optimum CM ratio and MR ratio were used for the vinyl acetate polymerization with the optimum RC. In order to ease sampling for kinetic measurement, the lowest possible MR area to MV ratio has been used. The polymerization was carried out as previously described (section 2.3). Using decane as an internal standard, 0.1 ml of the organic phase was taken at different time intervals and was used to determine the amount of the remaining vinyl acetate monomer. The experiment was conducted at 25 ℃, 35 ℃, 48 ℃, and 60 ℃. The controlling mechanism of the polymerization process was examined using the first-order and second-order kinetic models according to equations 6 and 7, respectively.

$$[A]_t = -k_1 t + [A]_o \quad (6)$$

$$1/[A]_t = k_2 t + 1/[A]_o \quad (7)$$

Where $[A]_o$ is the initial amount of vinyl acetate, $[A]_t$ is the amount of vinyl acetate remaining after time t, k_1 and k_2 are the first-order and second-order rate constant, respectively.
Similarly, the thermodynamic parameters (Activation energy E_A, enthalpy change ΔH, Gibb's free energy change ΔG, and entropy change ΔS) for polymerization were determined from the Arrhenius equation (8), Eyring equation (9), and Gibbs Helmholtz equation (10).

$$ln\ K_{obs} = ln\ A - \frac{E_A}{RT} \quad (8)$$

$$ln\left(\frac{K_{obs}}{T}\right) = \frac{\Delta H}{RT} + ln\left(\frac{k_g}{h}\right) + \frac{\Delta S}{R} \quad (9)$$

$$\Delta G = \Delta H - T\Delta S \quad (10)$$

Where K_{obs}, A, R, k_g, h, and T are the observed rate constant, pre-exponential factor, the universal gas constant, Boltzmann constant, Planck's constant, and the absolute temperature, respectively.

2.6. Catalyst recyclability/reusability study

Following the first run of polymerization under the optimum reaction conditions, the recyclability test was performed by separating the catalyst from the reaction mixture and washing with acetone to remove any bound PVAc. It was then dried in an oven at 60 ℃ for 2 h and reused for six cycles of vinyl acetate polymerization, repeating the separation, washing, and drying after each run. The percentage conversions of monomer after 12 h of each cycle were compared.

3.0. Results and discussion

3.1. Synthesis and characterization

Chit-Co(II), Chit-Ni(II), Chit-Mn(II) were synthesized by suspending chitosan in the respective metal ion solutions to allow complex formation as shown in scheme 1a. However, chitosan is

soluble in $Fe(NO_3)_3$ aqueous solution; thus, synthesis of Chit-Fe(III) was carried out by mixing chitosan and the metal ion solution as shown in scheme 1b. The resulting solution was allowed to dry and characterized along with the Chit-Co(II), Chit-Ni(II), and Chit-Mn(II) using UV-visible spectroscopy, FT-IR spectroscopy, X-ray diffraction (XRD) spectroscopy, H_2-TPR, thermal analysis, SEM-EDS, and ICP-OES.

Figure S2 (Supplementary Information) shows the UV-visible spectrum of Chitosan, Chit-Fe(III), Chit-Mn(II), Chit-Co(II), and Chit-Ni(II). No absorption band was observed in the spectrum of chitosan between the region of 200 – 800 nm, indicating a high degree of deacetylation. However, all the synthesized chitosan-metal coordination biopolymers revealed absorption bands in the UV-visible region, confirming the incorporation of metals into the chitosan biopolymer. The absorption bands have been assigned based on the coordination number of six. The absorption bands in the Chit-Fe(III) were assigned as follows: $^6A_{1g} \rightarrow {}^4T_{1g}$ (590 nm), $^6A_{1g} \rightarrow {}^4T_{2g}$ (G) (435 nm), $^6A_{1g} \rightarrow {}^4E_g$ (412 nm), $^6A_{1g} \rightarrow {}^4A_{1g}$, and the absorption band at 307 nm was assigned to a charge transfer. These absorption bands are weak and appear to overlap in the spectrum. Similarly, the absorption bands in the UV-Visible spectrum of Chit-Mn(II) at 629 nm and 336 nm were assigned to the $^6A_{1g} \rightarrow {}^4T_{1g}$ and charge transfer, respectively. In the same vein, Chit-Co(II) shows three weak absorption bands in the Visible region at 600 nm, 490 nm, and 409 nm; These have been assigned to the $^3T_{1g}$ (F) $\rightarrow {}^3T_{2g}$, $^3T_{1g}$ (F) $\rightarrow {}^3T_{1g}$ (P) and $^3T_{1g}$ (F) $\rightarrow {}^3A_{2g}$ respectively. Also, Chit-Ni(II) shows two absorption bands in the visible region at 648 nm and 386 nm, which we assign to the $^3A_{2g} \rightarrow {}^3T_{2g}$ and the $^3A_{2g} \rightarrow {}^3T_{1g}$ (F), respectively.

The FT-IR spectra of Chitosan, Chit-Mn(II), Chit-Ni(II), Chit-Co(II), and Chit-Fe(III) are shown in figure S3 (Supplementary Information). There is no major change in the skeletal backbone of chitosan after coordination with the metals, but a few minor changes were observed with the overlapping O-H and NH_2 stretching vibration at 3317 cm^{-1} as well as the C-H stretching vibration at 2887 cm^{-1} in chitosan. These minor changes are an indication of the formation of chitosan coordination biopolymers of the respective metal. In the spectrum of Chit-Mn(II), a hypochromic effect was observed with the -NH_2 and C-H stretching vibration. A similar occurrence was observed in the Chit-Ni(II) but with the total disappearance of the C-H vibration. The overlapping -NH_2 and O-H stretching vibration in chitosan underwent a redshift from 3317 cm^{-1} to 3280 cm^{-1} in the Chit-Co(II) while it broadens and overlaps with the

C-H stretching vibration in the Chit-Fe(III). All these changes suggest coordination between the metals and chitosan at the -OH and -NH_2 functional groups.

Figure S5 (Supplementary Information) shows the powdered X-ray diffractogram of chitosan, Chit-Mn(II), Chit-Ni(II), Chit-Co(II), and Chit-Fe(III). The weak broad peak and the intense broad peak at a diffraction angle of 10º and 22º respectively in the diffractogram of chitosan have been attributed to the semi-crystalline nature of chitosan [50] [60] while the sharp diffraction peaks at 37º and 43º correspond to the crystalline domain of chitosan. Upon coordination with metal ions, significant changes were observed. The crystallinity decreases in the order: Chit-Mn(II) > Chit-Co(II) > Chit-Ni(II) > Chit-Fe(III) with Chit-Mn(II) retaining a significant part of the crystalline domain whereas crystallinity vanished completely in the Chit-Fe(III).

The TGA (I) and DTA (II) curves of Chitosan, Chit-Co(II), Chit-Fe(III), Chit-Mn(II), and Chit-Ni(II) are shown in figure S12 (Supplementary Information). Except for Chit-Fe(III), all the TGA curves revealed two degradation stages. The first degradation step occurs at around 50 – 250 ℃, which is attributed to the elimination of hydrogen-bonded water molecule [58]; it is important to note that the amount of the hydrogen-bonded water molecule in chitosan and the coordination biopolymers is of the order: Chitosan < Chit-Co(II) < Chit-Mn(II) = Chit-Ni(II) based on the percentage weight loss in this temperature range. The main degradation stage (second degradation step) of chitosan and the coordination biopolymers starts at around 250 ℃; this is evident from the strong exothermic peaks observed at this temperature in the DTA curves of chitosan and the coordination biopolymers. However, after 450 ℃, the percentage weight loss of chitosan remains constant, but the percentage weight loss of the coordination biopolymers only remains fairly constant. Considering the overall percentage weight loss with respect to temperature, It can be inferred that the thermal stability is of the order: Chit-Co(II) > Chitosan > Chit-Mn(II) = Chit-Ni(II). On the other hand, four degradation steps were seen in the TGA curve of Chit-Fe(III) (figure S12c(I)). The first thermal degradation step has been assigned to the elimination of hydrogen-bound water molecules; this step occurs from 25 – 120 ℃ with about 6.5% weight loss. Thus, the amount of the hydrogen-bonded water molecule in the Chit-Fe(III) is less compared to the other coordination biopolymers [i.e Chitosan < Chit-Fe(III) < Chit-Co(II) < Chit-Mn(II) = Chit-Ni(II)]. The second degradation stage (between 120 – 150 ℃) may be due to chemical changes occurring in the coordination polymer. The main polymer decomposition is assumed to begin at 150 ℃ with an additional degradation step

around 623 ℃ which we also attributed to a chemical change in the coordination biopolymer. All the degradation steps in the Chit-Fe(III) were supported by the exothermic peaks revealed in the DTA curve. Also, as seen in figure S12, the thermal behavior of Chit-Fe(III) differs significantly from chitosan and the other coordination biopolymers. Based on the percentage weight loss with respect to temperature, it is clear that the order of thermal stability is: Chit-Co(II) > Chitosan > Chit-Mn(II) = Chit-Ni(II) > Chit-Fe(III).

Although the vinyl acetate polymerization reaction is aimed at ambient temperature, the tendency of the coordinated metal ions to be reduced with respect to temperature was investigated by Hydrogen-temperature-programmed reduction (H_2-TPR), and the result obtained is displayed in figure S4 (Supplementary Information). Only Chit-Fe(III) was reduced at the studied temperature range, specifically at 120 ℃ (sharp TCD signal assigned to $Fe^{3+} \rightarrow Fe^{2+}$) and 623 ℃ (weak TCD signal which may be due to the reduction of Fe^{2+} to Fe^{0}). This result is further supported by the TGA, and DTA analysis of the coordination biopolymers in figure S12 as only the Chit-Fe(III) shows a drastic decomposition at around 120 ℃, which cannot be taken as elimination of water molecule; a small degradation step and an exothermic peak were also respectively observed at around 623 ℃ in the TGA and DTA curve of Chit-Fe(III). There was no noticeable peak/TCD signal in the H_2-TPR of Chit-Ni(II), Chit-Co(II), and Chit-Mn(II); the TGA and DTA analysis also confirm this as the TGA and DTA curves of Chit-Ni(II), Chit-Co(II) and Chit-Mn(II) are well similar to the TGA and DTA curves of chitosan. This shows that the coordinated metal ions [Ni(II), Co(II), and Mn(II)] were not reduced in the studied temperature range.

The SEM micrographs of Chitosan, Chit-Co(II), Chit-Fe(III), Chit-Mn(II), and Chit-Ni(II) are shown in the supplementary information fig S6, S7, S8, S9, and S10, respectively. Upon coordination of chitosan with the metals, significant changes were observed in the SEM image of chitosan. The SEM micrographs of Chit-Co(II) (fig. S7(I)), Chit-Mn(II) (fig. S9(I)), and Chit-Ni(II) (fig. S10(I)), which were prepared using the same method, show similar images, while the SEM micrograph of Chit-Fe(III) (fig. S8(I) Supplementary Information) appears odd. Chit-Fe(III) has a smooth surface since the gelly-like solution obtained after mixing Fe(III) salt with chitosan was air-dried to obtain a smooth film. In addition, the EDS spectral (fig. S6(II), S7(II), S8(II), S9(II), and S10(II)) confirms the successful incorporation of the metals into the chitosan biopolymer as significant counts of the metals were observed in each EDS spectrum.

Only the Chit-Ni(II) (fig. S10(II)) reveals the presence of trace elements (Ru and Si) which are probably present as impurities in the Ni(II) salt used.

The percentage anchored metal unto the chitosan biopolymer was determined using ICP-OES, and the result is presented in table 1. Chit-Fe(III) shows the highest metal content, and this is a reflection of the preparation procedure as there was no filtration. While the percentage of metal loading plays an important role in increasing the activity of the coordination biopolymer, the nature of the coordinated metal ion plays a dominant role. As seen in section 3.3, Chit-Fe(III), with the highest percentage metal loading, was inactive, and Chit-Mn(II), with the lowest percentage metal loading, was active towards vinyl acetate polymerization. However, the high activity of Chit-Co(II) over Chit-Mn(II) may not only be due to the nature of the metals but also the higher metal content in Chit-Co(II).

Table 1: Percentage of metal loadings on chitosan biopolymer

Entries	Coordination biopolymer	% metal loading
1	$\mathrm{Chit-Fe(III)}$	8.6552
2	$\mathrm{Chit-Ni(II)}$	5.7260
3	$\mathrm{Chit-Co(II)}$	6.0980
4	$\mathrm{Chit-Mn(II)}$	1.2037

3.2. Result of computational analysis

Figure 2 shows the structures of the pre-optimized four isomers of each coordination biopolymer, namely: Chit-Co(II) (fig. 2a), Chit-Mn(II) (fig. 2b), and Chit-Ni(II) (fig. 2c). In isomers I, two chlorides are *trans* to the -OH and -NH_2 donor sites of chitosan. In isomers II, the chlorides are *trans* to each other. In isomers III, one of the chlorides is *trans* to the –OH donor site of chitosan, while in isomers IV, one of the chlorides is *trans* to the –NH_2 donor site of chitosan.

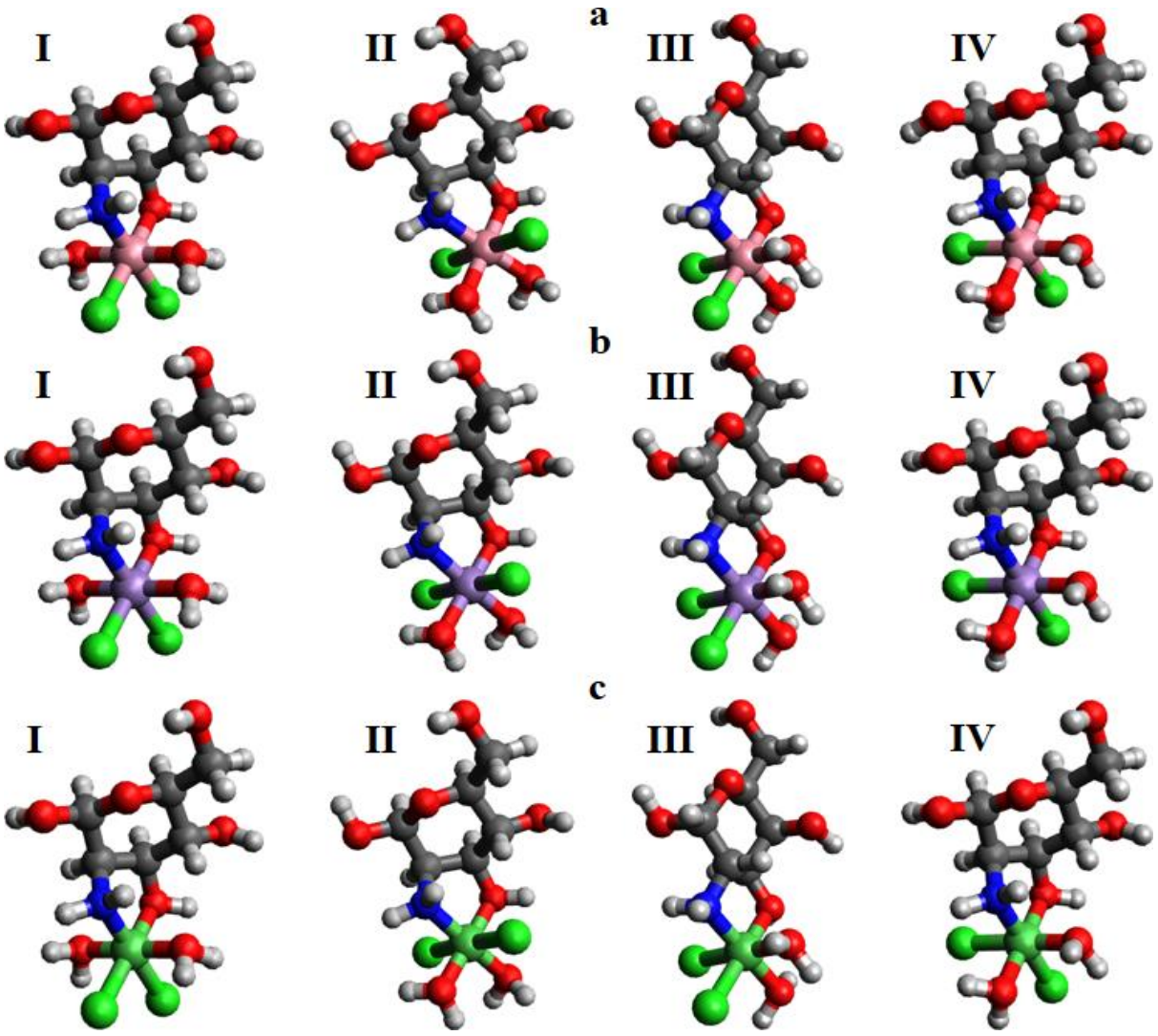

Figure 2: Pre-optimized four isomers structure of (a) Chit-Co(II) (b) Chit-Mn(II) (c) Chit-Ni(II)

The result of the final single point energy for each of the isomers obtained from geometry optimization at the BP-RI/def2-SVP level of theory using ORCA is depicted in table 2. The optimized structure and the geometry convergence of the isomers for the coordination biopolymers are shown in figure 3 [for Chit-Ni(II)], figure S13, and figure S14 in the supplementary information for Chit-Co(II) and Chit-Mn(II), respectively. As seen in table 2, Isomer II (where the two chlorides are *trans* to each other) is the most stable configuration for each of the coordination biopolymers. The HOMO and LUMO orbital diagram of the Chit-unit, Chit-Fe(III), as well as the most stable isomer of Chit-Co(II), Chit-Mn(II), and Chit-Ni(II), are displayed in figure 4, while their HOMO – LUMO energy values are shown in table 3. The HOMO – LUMO energy gap of the Chit-unit is lowered after coordination with the metals, as seen in table 3. Also, the HOMO – LUMO energy gap of each coordination biopolymer appears to affect the polymerization efficiency, as discussed in section 3.3.1.

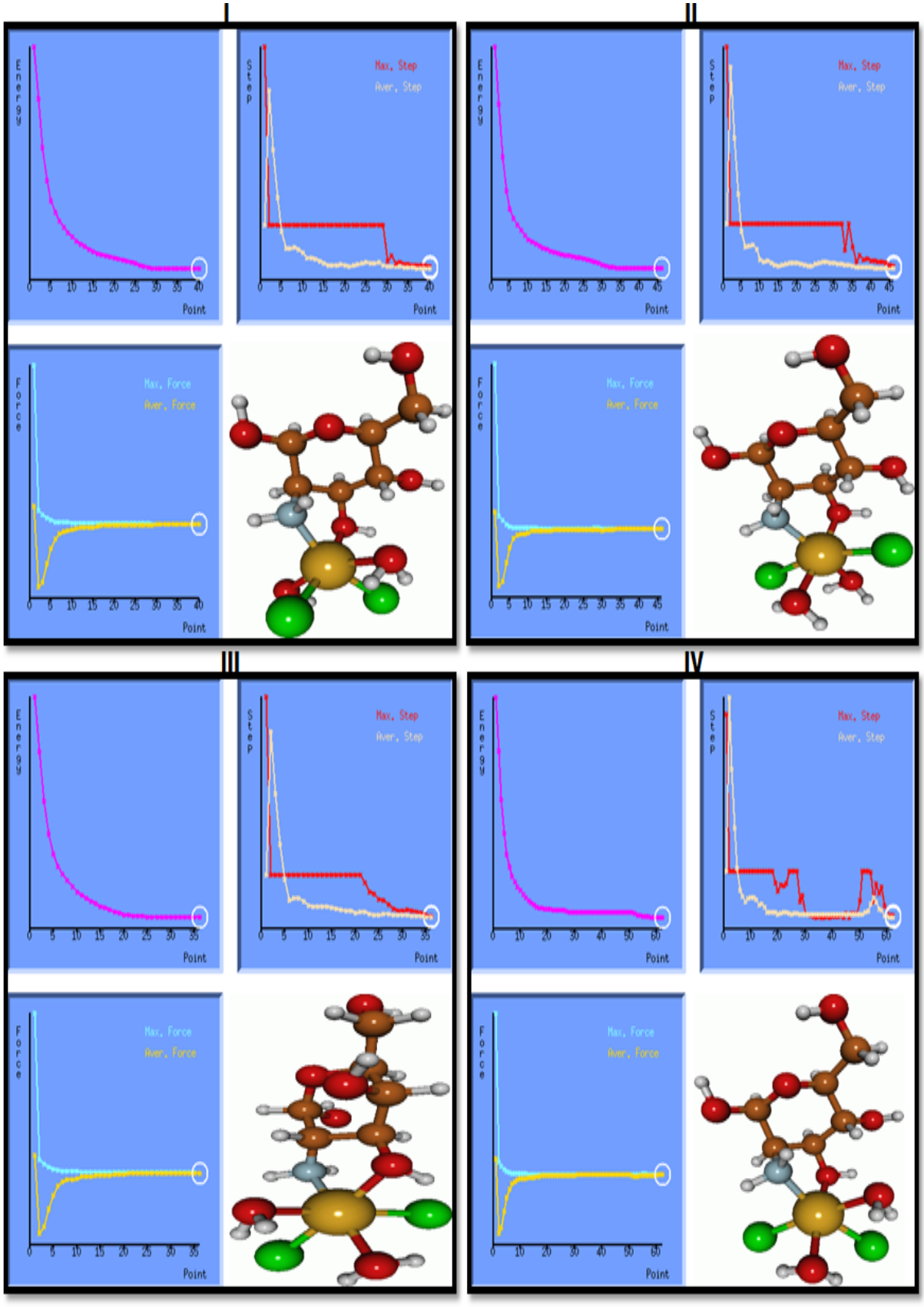

Figure 3: Optimized structures and geometry convergence of the four isomers of Chit-Ni(II)

3.3. Polymerization of vinyl acetate

When the coordination biopolymers were used as catalyst/initiator as discussed in section 2.3, only Chit-Mn(II) and Chit-Co(II) initiate the polymerization process giving a percentage conversion of 25% and 52% respectively after 24 h whereas Chit-Ni(II) and Chit-Fe(III) were inactive under the polymerization condition as shown in figure 1. The PVAc produced from Chit-Mn(II), and Chit-Co(II) were analyzed using FT-IR, and the results were compared with a commercial PVAc bead obtained from a manufacturer (Sigma Aldrich), as shown in figure 5a. The PVAc produced from Chit-Co(II) compares well with the PVAc obtained from the manufacturer. Therefore more PVAc was produced with Chit-Co(II) and further compared with the PVAc bead from the manufacturer using UV-visible spectroscopy (fig. 5b), ^{1}H NMR spectroscopy (Supplementary Information fig. S11), and SEM-EDS (fig. 6 and 7). A perfect comparison was obtained with the UV-visible spectroscopy (fig. 5b) and ^{1}H NMR spectroscopy (fig. S11)). However, the EDS spectra revealed the presence of minor impurities (namely: Ca, S, Si, and K) in the PVAc produced from Chit-Co(II), as evident from Figures 6 and 7. Ca would have originated from the Chit-Co(II) and more specifically, from chitosan due to incomplete demineralization of crab shell as seen in the EDS spectrum of chitosan (Supplementary Information fig. S6(II)). Undoubtedly, S emanates from the reducing agent (Na_2SO_3(aq)) during the polymerization process. Si and K could be trace elements present in one or more of the reagents used in the polymerization process.

Table 2: Result of the final single point energies for the four isomers of the coordination biopolymers

Coordination biopolymer	Final Single Point energy of Isomer I (Eh)	Final Single Point energy of Isomer II (Eh)	Final Single Point energy of Isomer III (Eh)	Final Single Point energy of Isomer IV (Eh)
Chit-Co(II)	-3122.6320	-3122.7734	-3122.6448	-3122.6414
Chit-Mn(II)	-2890.8562	-2890.9139	-2890.8910	-2890.8920
Chit-Ni(II)	-3248.1814	-3248.1987	-3248.1820	-3248.1729

Theoretically, based on the chemical environment and neglecting the chain end, polyvinyl acetate contains three types of protons, namely, methylene (-CH_2-) protons of the alcohol unit, methine (>CH-) protons in the acetate and alcohol unit, and methyl (-CH_3) protons of the acetate group. All these three protons are indicated with the colour red in figure 8. The ^{1}H NMR of the synthesized material revealed distinct peaks that correspond to the chemical shift values of the protons in polyvinyl acetate. Thus, confirming the successful one-pot synthesis of polyvinyl acetate using the Chit-Co(II) as a catalyst. As shown in figure 8, the proton peaks have been assigned as follows:

Methylene proton of alcohol unit: 1.706 δ, 1.797 δ; methyl proton of the acetate unit: 1.968 δ; methine proton in acetate and alcohol unit: 4.813 δ.

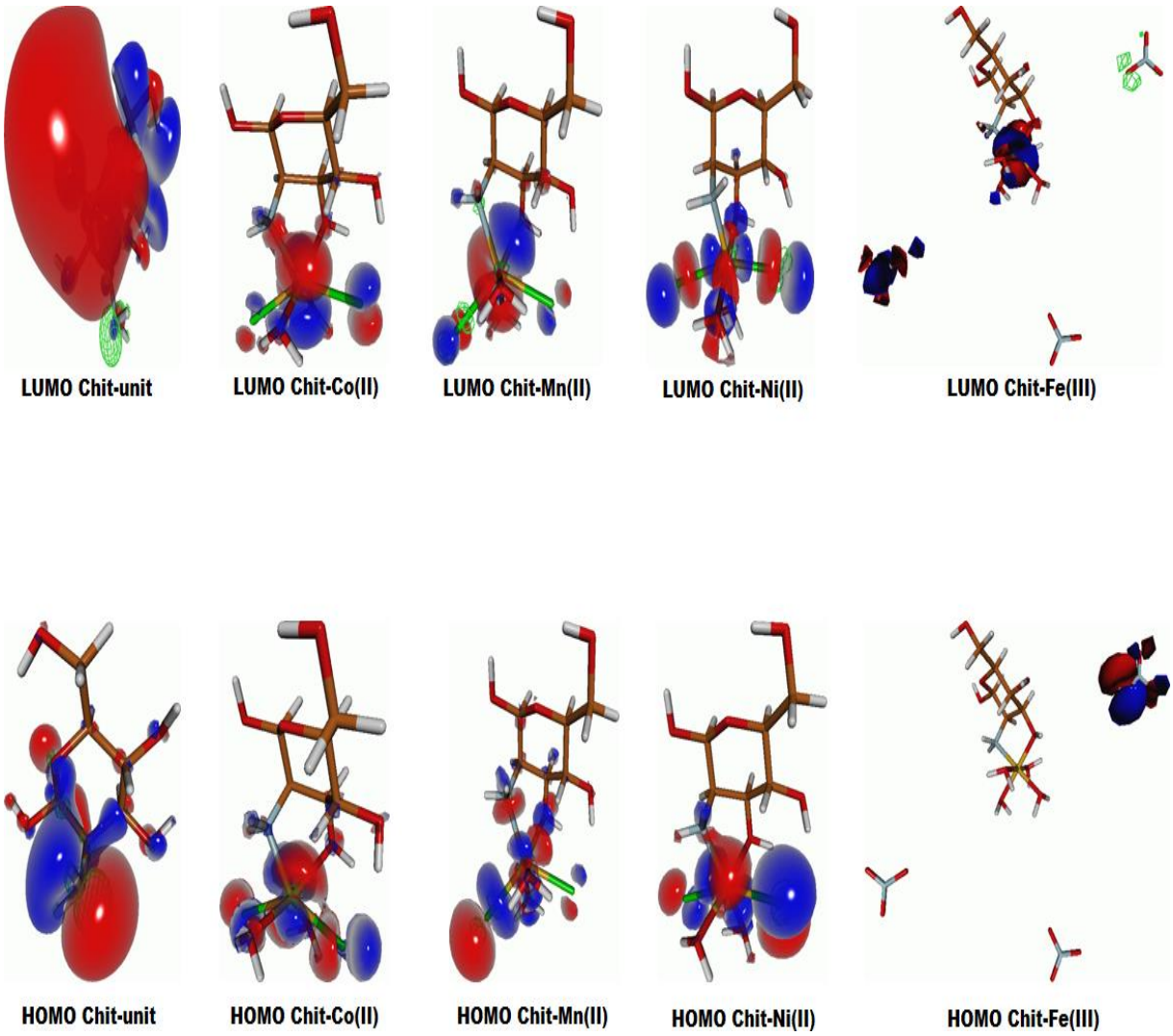

Figure 4: HOMO and LUMO orbital diagram of Chitosan monomer unit and the coordination units [Chit-Co(II), Chit-Mn(II), Chit-Ni(II), and Chit-Fe(III)]

Similarly, in addition to peaks due to methine (>CH-) carbon, methylene (-CH_2-) carbon, and the methyl (-CH_3) carbon, there is a carbonyl (>C=O) carbon whose peak is expected in the ^{13}C NMR spectrum of polyvinyl acetate. As anticipated, the peaks due to all these four carbons (>CH-, -CH_2-, -CH_3, and >C=O) are clearly seen in the ^{13}C NMR spectrum of the synthesized material (fig. 9). This further gives convincing evidence that PVAc has been successfully produced with the use of the Chit-Co(II) as the catalyst. From figure 9, it can be argued that all the methyl (-CH_3) carbons in the synthesized PVAc overlap at 21.17 δ, the methylene (-CH_2-) carbons overlap between 27.30 - 40.12 δ, the methine (>CH-) carbons overlap between 66.67-68.15 δ, and the carbonyl (>C=O) carbons overlap at 170.51 δ.

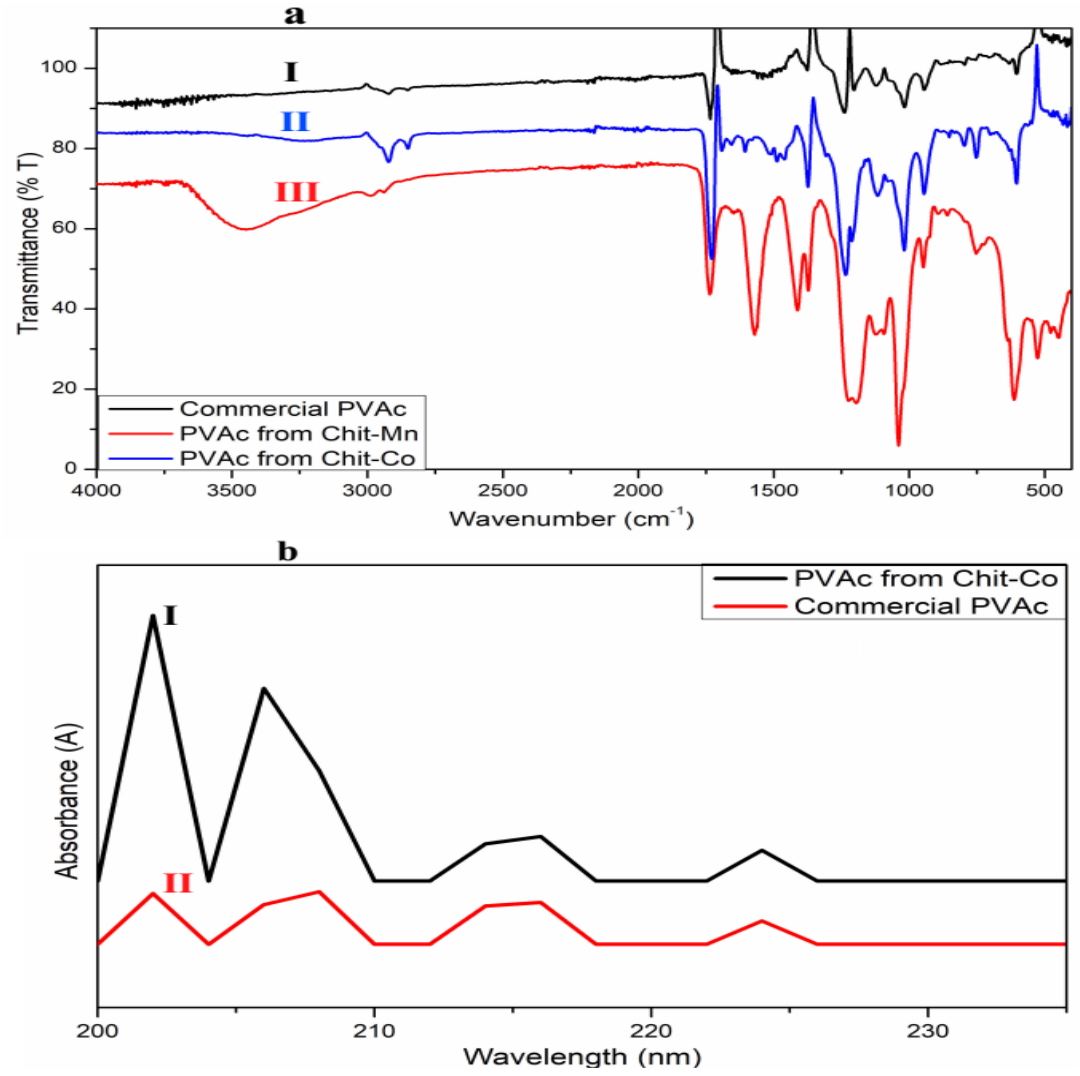

Figure 5: (a) FT-IR spectrum of (I) Commercial PVAc (II)PVAc produced from Chit-Co(II) (III) PVAc produced from Chit-Mn(II); (b) UV-visible spectrum of (I) PVAc produced from Chit-Co(II) (II) Commercial PVAc

Figure S15 (Supplementary Information) shows the plot of reduced viscosity and inherent viscosity against the concentration of the PVAc solution. The common ordinate (intrinsic viscosity) of the two graphs was found to be 0.015 $l \cdot g^{-1}$ and was used to determine the viscosity average molecular weight (M) of the synthesized PVAc according to Mark-Houwink equation described in the experimental section 2.3. The viscosity average molecular weight (M) was obtained as M = 25,078.

3.3.1. Mechanism of vinyl acetate polymerization

The proposed mechanism of vinyl acetate polymerization using Chit-Co(II) as catalyst/initiator is illustrated in scheme 2. Na_2SO_3(aq), being a reducing agent, releases electrons at the interface between the aqueous and organic layer. The electron reduces each neutral coordination complex of Co(II) in the coordination polymer sitting at the aqueous-organic interface to an anionic complex. The anions generated are transferred to the chain end as vinyl acetate combines with the complexes, and chain propagation continues as more vinyl acetate combines. Chain termination occurs either by disproportionation or combination between two adjacent growing chains. The equilibrium set up in the generation of an electron makes it a controlled living polymerization.

However, if the Co(II) is reduced to Co^0 in the coordination complexes, then the propagation proceeds via the transfer of two negative charges. The same mechanism applies to Chit-Mn(II). Since the anionic charges are generated on the surface of the Chit-M(II), and the chain initiation occurs on the surface of the Chit-M(II), the polymerization process would be said to have occurred via surface-initiated atom transfer radical polymerization (SI-ATRP). The results obtained from the computational study further support the observed trend in the yield of polymerization using the coordination biopolymers [Chit-Co(II), Chit-Mn(II), Chit-Fe(III), and Chit-Ni(II)]. The reduction potential of the coordination complexes is greatly influenced by the HOMO – LUMO energy gap. The Chit-Co(II) with the lowest HOMO – LUMO energy gap of 0.6685 eV was easily reduced and gave the highest percentage yield, followed by the Chit-Mn(II) with a HOMO – LUMO energy gap of 1.0374 eV. Chit-Fe(III) and Chit-Ni(II) with HOMO – LUMO energy gap of 1.5848 eV and 2.5634 eV respectively could not initiate the polymerization process under the same condition due to higher reduction potential.

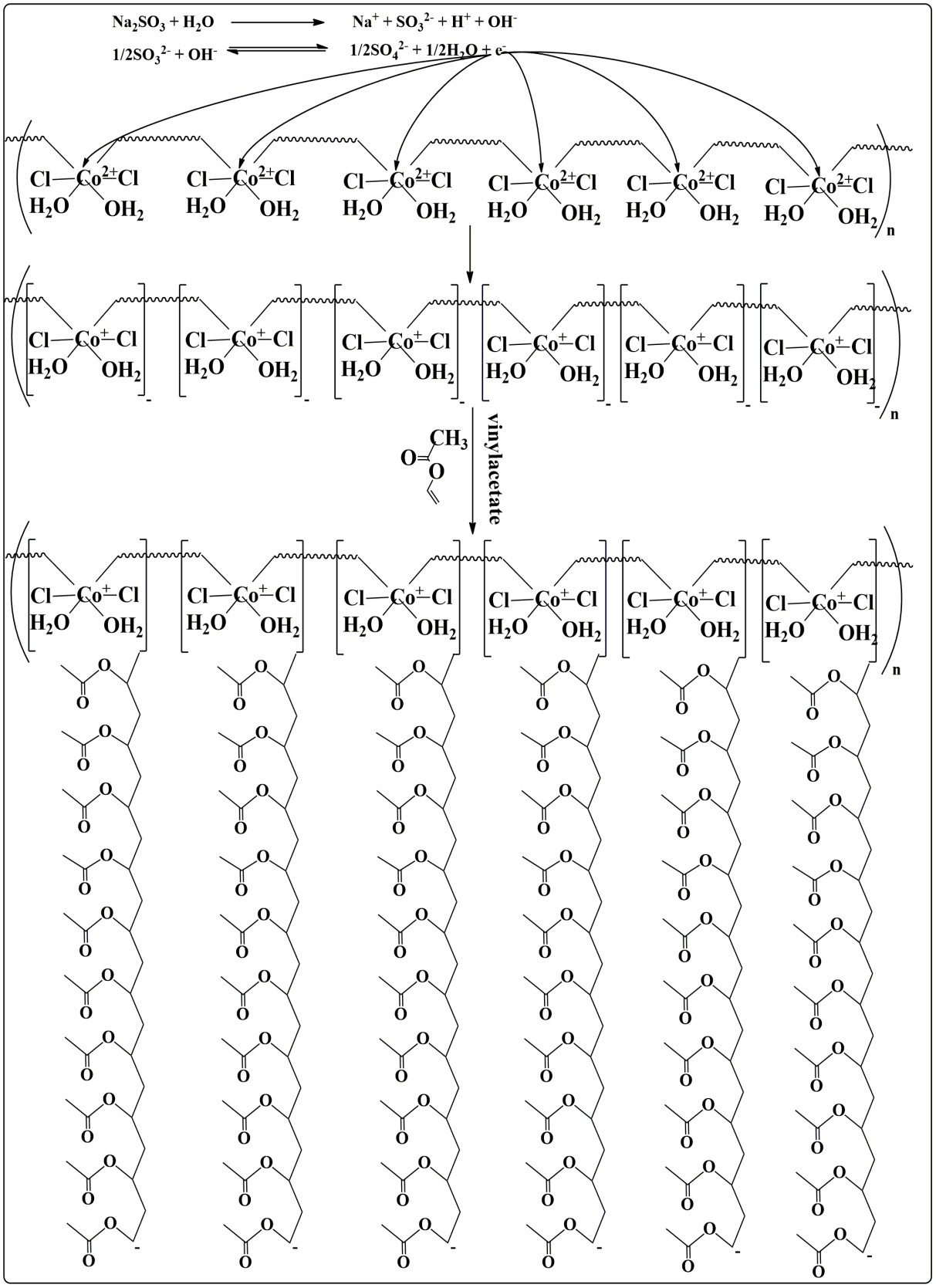

Scheme 2: Proposed mechanism of vinyl acetate anionic polymerization using chit-Co(II) in the presence of aqueous sodium sulphite via interfacial electron transfer

Table 3: HOMO – LUMO energy values of chitosan monomer [N-acetyl glucosamine] unit and the coordination units [Chit-Co(II), Chit-Mn(II), Chit-(Ni(II), and Chit-Fe(III)]

S/N	Material	HOMO energy (eV)	LUMO energy (eV)	HOMO-LUMO energy gap (eV)
1	Chit-unit	-4.9028	0.2024	5.1052
2	Chit-Co(II)	-3.2515	-2.5830	0.6685
3	Chit-Mn(II)	-2.1807	-1.1433	1.0374
4	Chit-Ni(II)	-4.1088	-1.5454	2.5634
5	Chit-Fe(III)	0.02740	1.61116	1.5848

3.4. Reaction optimization

3.4.1. Effect of CM ratio

Figure 10a shows the effect of catalyst amount (in gram) per 1 ml of monomer liquid on the yield of polyvinyl acetate. It is evident that there is no major increase in the percentage conversion of monomer when the catalyst amount is increased beyond 0.01 g. Hence, the catalyst to monomer ratio can be kept at 0.01 g/ml without undermining the polymer yield.

3.4.2. Effect of RC

The effect of reducing agent (Na_2SO_3(aq)) concentration (RC) is illustrated in figure 10b. The percentage of monomer conversion increases as RC increases until a maximum at around 1.6 M after which a decrease in monomer conversion begins. Notably, the maximum solubility of Na_2SO_3 at 20 ℃ is 27.0 g/100 ml (about 2.1 M). It appears that the chain initiation process is endothermic in nature, as some precipitate of $Na_2SO_{3(s)}$ were seen before polymerization begins when a concentration of 2.0 M was used. In essence, the heat was absorbed from the aqueous phase during the chain initiation, and this was compensated for by the precipitation of Na_2SO_3(s) over a period of time before polymerization begins, which is a reason for the

decrease in monomer conversion with time. However, no such precipitation was observed with a concentration of 1.6 M and below.

3.4.3. Effect of MR ratio

Ordinarily, the Monomer-Reducing agent ratio (MR ratio) was not conceived to affect the yield of vinyl acetate polymerization as the process occurs at the monomer-aqueous interface. However, since the polymer grows through the aqueous phase, an optimum aqueous volume is required to prevent rapid chain termination. The effect of the MR ratio on the yield of polyvinyl acetate after 12 and 24 h is shown in figure 10c, and the optimum monomer-reducing agent (MR ratio) was found to be 1:3.

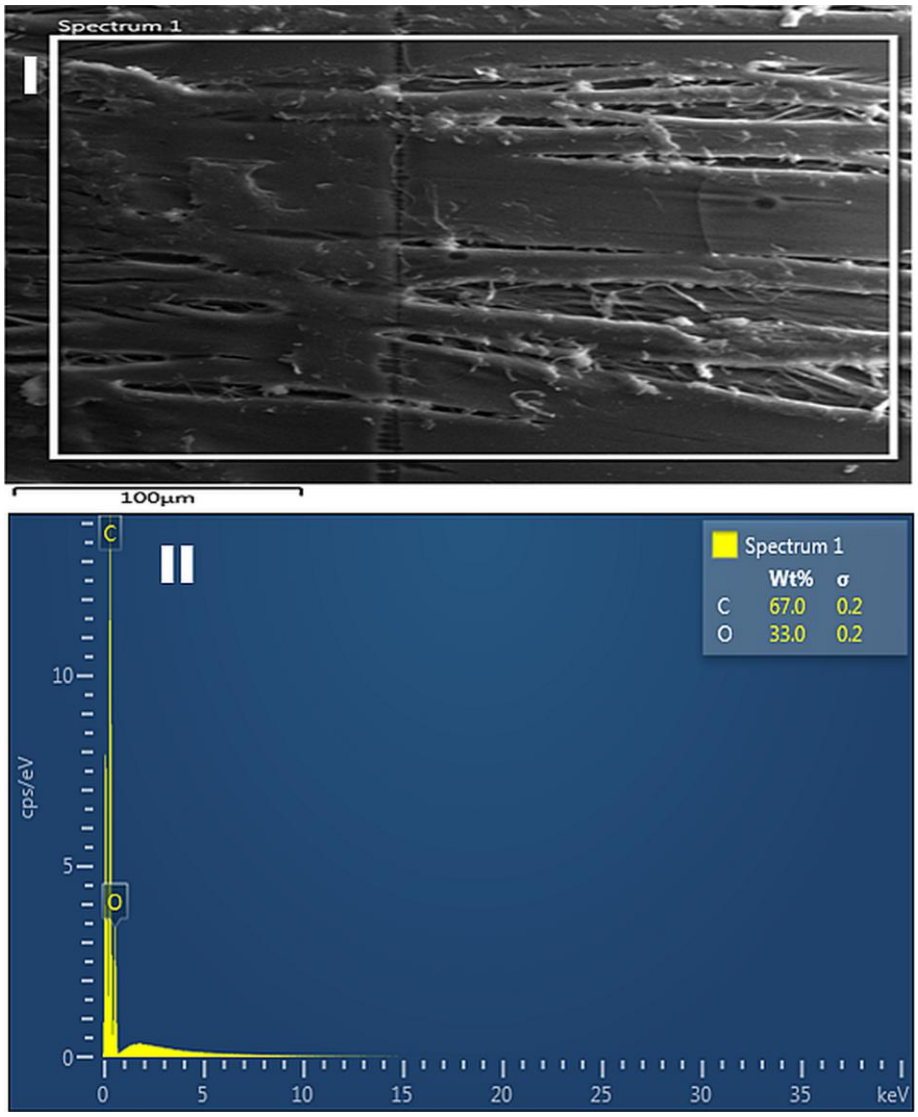

Figure 6: (I) SEM micrograph of Commercial PVAc (II) EDS of Commercial PVAc

3.4.4. Effect of MR area to MV ratio

Figure 10d illustrates the effect of the Monomer-Reducing agent contact area (MR area) to monomer volume (MV) ratio after 9 and 11 h of polymerization of vinyl acetate. It can be seen that the higher the MR area to MV ratio, the higher the rate of percentage monomer conversion. However, for the analytical purpose, the MR area to MV ratio can be kept moderate for easy sampling of the organic phase.

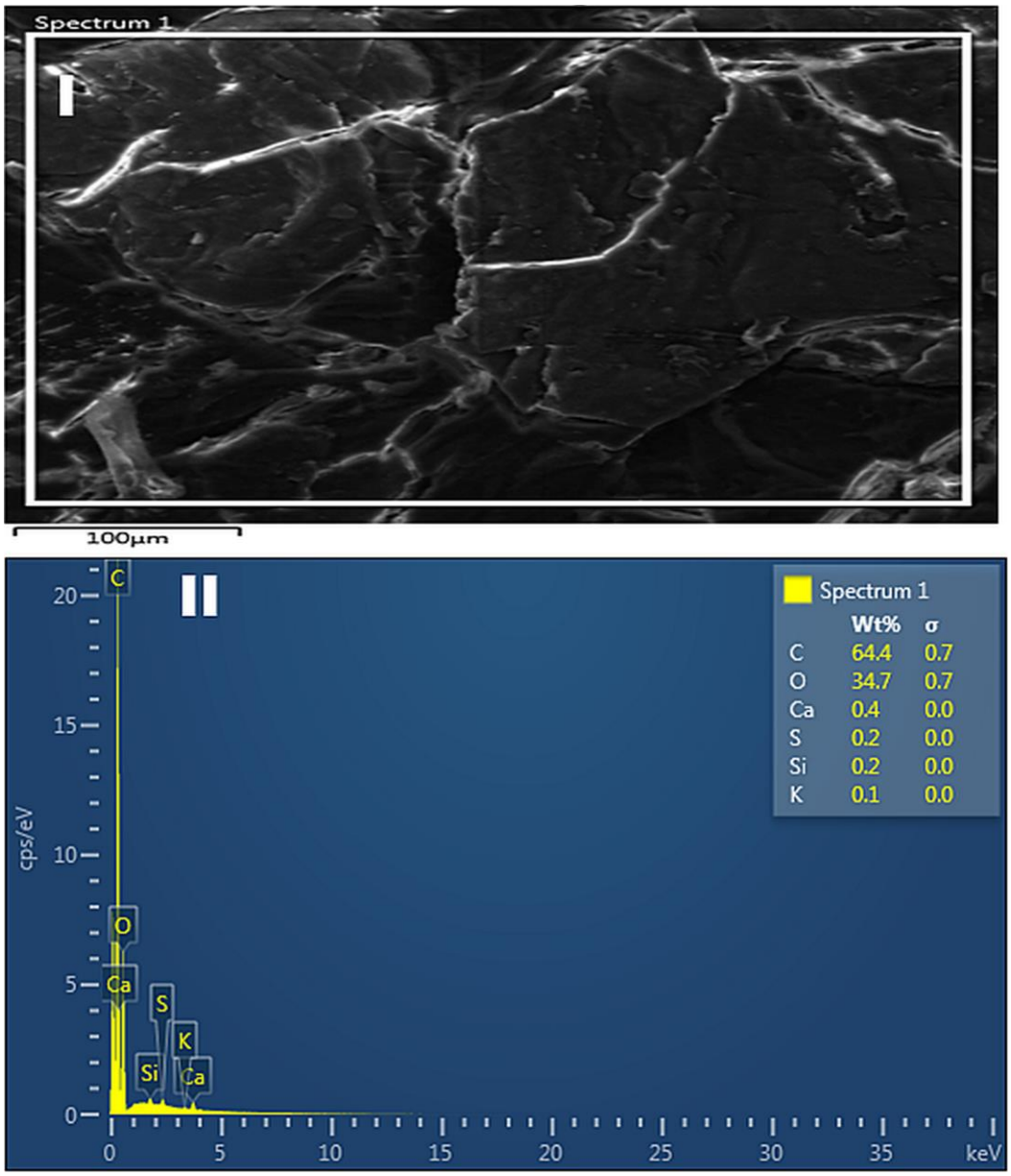

Figure 7: (I) SEM micrograph of PVAc produced from Chit-Co(II) (II) EDS spectrum of PVAc produced from Chit-Co(II)

3.5. Catalyst reusability

The result of the catalyst recyclability test is shown in figure 10e. No change in catalyst activity was observed after seven cycles of polymerization. The result shows that the catalyst system can be used for several polymerization cycles. However, the catalyst color (purple) changes completely to brown after about 3 – 4 cycles without a loss of activity; this is probably due to the reduction of Co(II) to a lower oxidation state in the Chit-Co(II).

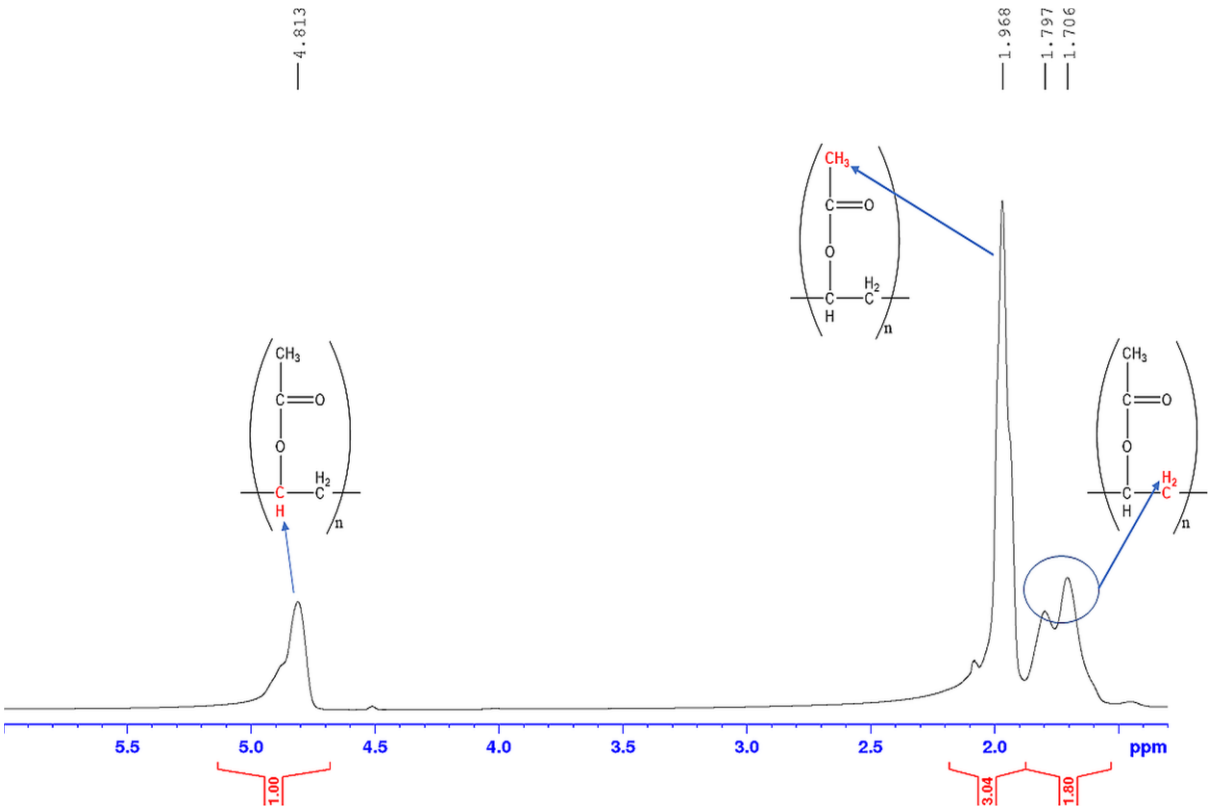

Figure 8: ^{1}H NMR of the polyvinyl acetate (PVAc) produced from Chit-Co(II)

3.6. Result of kinetics and thermodynamic studies

The kinetics and thermodynamic plots are displayed in figure S16 (Supplementary Information). Figure S16a shows the linear plot of $[A]_t$ against t at varying temperatures, while figure S16b shows the plot of $1/[A]_t$ against t at varying temperatures; k_1 and k_2 were obtained from the slopes in figure S16a and S16b respectively. The rate of vinyl acetate polymerization was found to depend on both the amount of vinyl acetate and Chit-Co(II) catalyst at ambient

temperature (25 ℃) (i.e., the polymerization process fitted well with a second-order kinetic model at 25 ℃) while the polymerization process can best be described with the first-order kinetic model at elevated temperature; this is evident from the linear correlation coefficients illustrated in table 4. Figure S16c and S16d show the Arrhenius plots [i.e., graph of ln k_{obs} against 1/T] while the Eyring's plots [i.e., the graph of ln (k_{obs}/T) against 1/T] are shown in figure S16e and S16f. From the slopes and intercepts coupled with the Gibbs Helmholtz equation (10), the activation parameters were calculated and presented in table 5. The high activation energy E_A indicates that the chain initiation process is endothermic, as suggested in section 3.4.2. The heat was absorbed from the surrounding aqueous solution to overcome the activation energy leading to the precipitation of Na_2SO_3 at a concentration higher than 1.6 M. The negative value of ΔH shows that the chain propagation process is exothermic. In the same vein, the negative value of ΔS is an indication of a decrease in entropy as expected of a polymerization process where a liquid monomer (vinyl acetate) is converted to a solid polymer (polyvinyl acetate). Also, the negative value of ΔG shows that polymerization is a spontaneous process at ambient temperature.

Table 4: Correlation coefficients (R^2) and rate constants (k) obtained from the kinetic studies of vinyl acetate polymerization at varying temperatures using Chit-Co(II) as the catalyst.

Temperature (℃)	Kinetic model			
	First-order		Second-order	
	R^2	k_1	R^2	k_2
25	0,7187	5.9662	0.8747	0.0012
36	0.9434	9.9187	0.8420	0.0051
48	0.9187	10.0962	0.9060	0.0052
60	0.8297	12.0458	0.7018	0.0312

Table 5: Activation parameters of Chit-Co(II) for the polymerization of vinyl acetate base on the second-order rate constant.

Activation parameters	
E_A (KJ/mol)	68.7694
ΔH (KJ/mol)	-66.1523
ΔS (J/molK)	-78.2486
ΔG_{298} (KJ/mol)	-42.8342

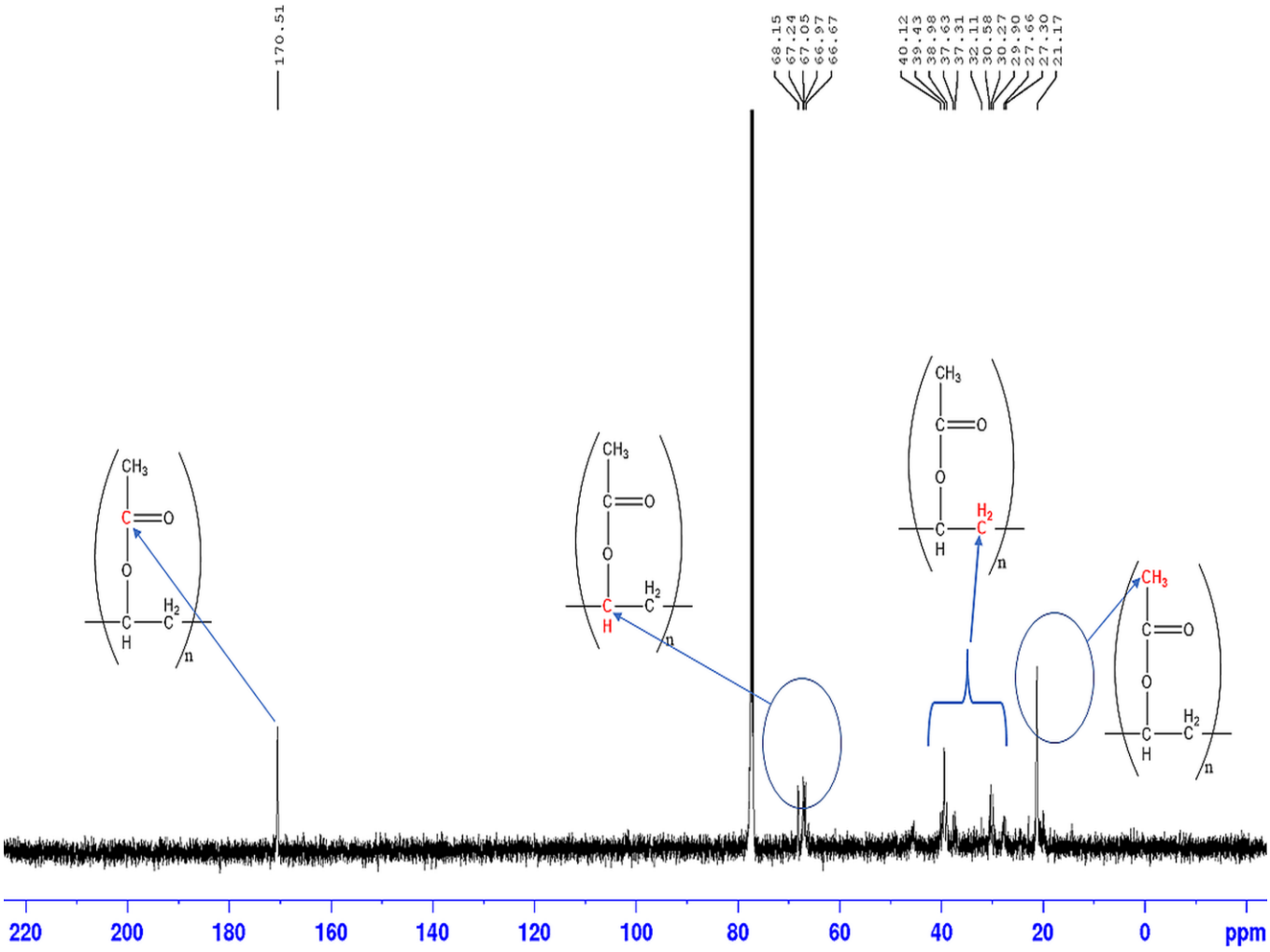

Figure 9: ^{13}C NMR of the polyvinyl acetate (PVAc) produced from Chit-Co(II)

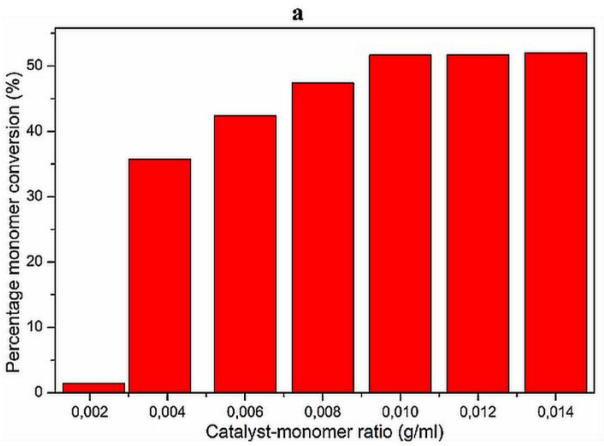

Reaction time = 24 h, reaction temperature = 25 °C, [Na_2SO_3] = 1M, VAc:Na_2SO_3 = 1vol/1vol, MR area/MV = 2.7786 cm^{-1}

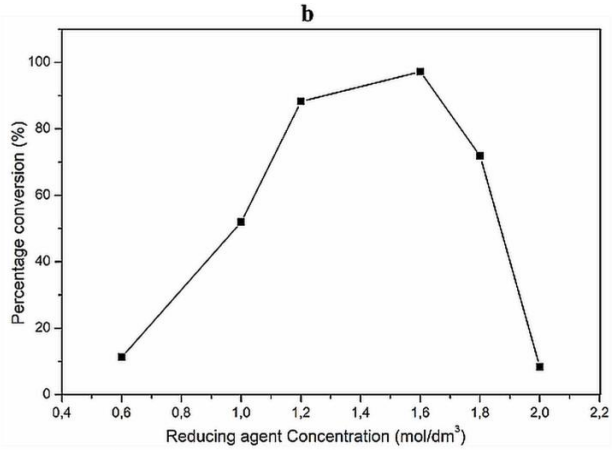

Reaction time = 24 h, reaction temperature = 25 °C, VAc:Na_2SO_3 = 1vol/1vol, Chit-Co:VAc = 0.01 g/ml, MR area/MV = 2.7786 cm^{-1}

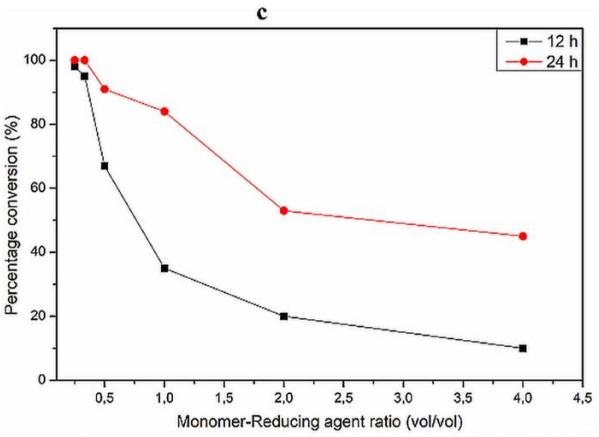

Reaction temperature = 25 °C, [Chit-Co]/[Vac] = 0.01 g/ml, [Na_2SO_3] = 1.6 M, MR area/MV = 2.7786 cm^{-1}

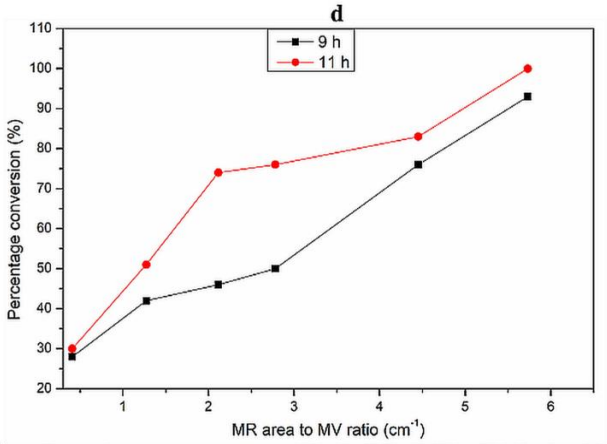

Reaction temperature = 25 °C, [VAc]/[Na_2SO_3]= 1vol/3vol, [Chit-Co]/[Vac] = 0.01 g/ml, [Na_2SO_3] = 1.6 M

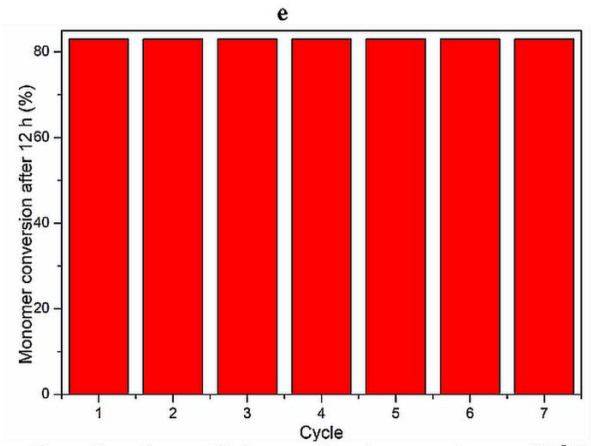

Reaction time = 12 h, reaction temperature = 25 °C
[VAc]/[Na_2SO_3] = 1 vol/3 vol, [Chit-Co]/[VAc] = 0.01 g/ml, [Na_2SO_3] = 1.6 M, MR area/MV = 4.4493 cm^{-1}

Figure 10: (a) Effect of catalyst-monomer ratio (CM ratio) (b) Effect of reducing agent concentration (RC) (c) Effect of monomer-reducing agent volume ratio (MR ratio) (d) Effect of monomer-reducing agent contact area (MR area) to monomer volume (MV) ratio € Chart of catalyst reusability/recyclability

4.0. Conclusion

The chitosan-metal coordination biopolymer of Mn(II), Fe(III), Co(II), and Ni(II) have been synthesized and characterized using different instrumental techniques, namely: UV-visible spectroscopy, FT-IR spectroscopy, X-ray diffraction (XRD) spectroscopy, H_2-TPR, thermal analysis (TGA and DTA), scanning electron microscopy – energy dispersive spectroscopy (SEM-EDS) and Inductively coupled plasma – optical emission spectroscopy (ICP-OES). Chit-Co(II) and Chit-Mn(II) have been found to be active towards vinyl acetate polymerization, with Chit-Co(II) exhibiting higher catalytic activity. Attempts towards understanding the mechanism of polymerization show that the chain propagation occurs through the transfer of radical anion and that the polymer grows from the surface of the Chit-Co(II) and Chit-Mn(II) catalysts. Hence, the surface-initiated atom transfer radical polymerization (SI-ATRP) process was suggested. The trend in the efficiency of the coordination biopolymers towards vinyl acetate polymerization has been linked to their respective HOMO – LUMO energy gaps. The viscosity average molecular weight of PVAc produced was measured as M = 25, 078. Based on the coordination number of six, the coordination orientation of the Chit-Co(II) has been ascertained using a density functional theory approach. Kinetic studies show that the vinyl acetate polymerization suits the second-order kinetic model at ambient temperature. Thermodynamic studies also revealed that chain initiation is an endothermic process while chain propagation is an exothermic process. Interestingly, there was no significant loss of activity for the Chit-Co(II) after seven cycles of polymerization. This makes Chit-Co(II) a promising catalyst for vinyl acetate polymerization necessitating the need for further improvement, perhaps through chemical modification of chitosan before coordinating with Cobalt. Nonetheless, the catalytic activities of the chitosan coordination biopolymers of other row transition metals bearing similar electronic configuration with Cobalt may also be explored in this regard. A biomedical application is also possible by examining the chitosan-metal coordination biopolymer using the low-ppm ATRP approach.

5.0. Conflicts of interest

There are no conflicts to declare

6.0. Acknowledgment

The financial assistance of The World Academy of Sciences (TWAS) in collaboration with the National Research Foundation (NRF) and the Department of Science and Technology (DST) of the Republic of South Africa towards this research is hereby acknowledged. Opinions expressed and conclusions arrived at are those of the authors and are not necessarily to be attributed to the DST-NRF-TWAS.

Supplementary Information

References

[1] R. B. N. Baig, M. N. Nadagouda and R. S. Varma, Green Chemistry 16 (2014) 2122.

[2] M. Lamblin, L. Nassar-Hardy, J. Hierso, E. Fouquet and F. Felpin, Advanced Synthesis & Catalysis 352 (2010) 33.

[3] M. Chtchigrovsky, A. Primo, P. Gonzalez, K. Molvinger, M. Robitzer, F. Quignard and F. Taran, Angewandte Chemie (International ed. in English) 48 (2009) 5916.

[4] J. Ma and Y. Sahai, Carbohydrate Polymers 92 (2013) 955.

[5] C. K. S. Pillai, W. Paul and C. P. Sharma, Progress in polymer science 34 (2009) 641.

[6] V. Zargar, M. Asghari and A. Dashti, ChemBioEng reviews 2 (2015) 204.

[7] J. Sun, J. Wang, W. Cheng, J. Zhang, X. Li, S. Zhang and Y. She, Green Chemistry 14 (2012) 654.

[8] R. S. Varma, Current Opinion in Chemical Engineering 1 (2012) 123.

[9] M. Lee, B. Chen and W. Den, Applied Sciences 5 (2015) 1272.

[10] R. B. N. Baig and R. S. Varma, Green Chemistry 15 (2013) 1839.

[11] Y. Inaki, M. Otsuru and K. Takemoto, Journal of Macromolecular Science: Part A - Chemistry 12 (1978) 953.

[12] Otsu, Takayuki., Yoshida, Masatoshi and Tazaki, Toshinori, Die Makromolekulare Chemie, Rapid Communication 3 (2003) 133.

[13] C. Boyer, N. A. Corrigan, K. Jung, D. Nguyen, T. Nguyen, N. N. M. Adnan, S. Oliver, S. Shanmugam and J. Yeow, Chemical reviews 116 (2016) 1803.

[14] K. Matyjaszewski, B. S. Sumerlin, N. V. Tsarevsky, J. Chiefari and American Chemical Society, Division of Polymer Chemistry Staff, Controlled Radical Polymerization: Mechanisms (American Chemical Society, Washington, DC, 2016).

[15] W. Tang and K. Matyjaszewski, Macromolecules 40 (2007) 1858.

[16] Y. Wang, Y. Kwak, J. Buback, M. Buback and K. Matyjaszewski, ACS Macro Letters 1 (2012) 1367.

[17] K. Matyjaszewski and N. V. Tsarevsky, Journal of the American Chemical Society 136 (2014) 6513.

[18] J. Morick, M. Buback and K. Matyjaszewski, Macromolecular Chemistry and Physics 213 (2012) 2287.

[19] Y. Zhang, Y. Wang, C. Peng, M. Zhong, W. Zhu, D. Konkolewicz and K. Matyjaszewski, Macromolecules 45 (2012) 78.

[20] M. Li and K. Matyjaszewski, Macromolecules 36 (2003) 6028.

[21] M. Li, N. M. Jahed, K. Min and K. Matyjaszewski, Macromolecules 37 (2004) 2434.

[22] M. Li, K. Min and K. Matyjaszewski, Macromolecules 37 (2004) 2106.

[23] K. Min, H. Gao and K. Matyjaszewski, Journal of the American Chemical Society 127 (2005) 3825.

[24] Y. Yamamura and K. Matyjaszewski, Journal of Macromolecular Science, Part A 44 (2007) 1035.

[25] W. Jakubowski and K. Matyjaszewski, Macromolecules 38 (2005) 4139.

[26] Y. Kwak, A. J. D. Magenau and K. Matyjaszewski, Macromolecules 44 (2011) 811.

[27] A. Simakova, S. E. Averick, D. Konkolewicz and K. Matyjaszewski, Macromolecules 45 (2012) 6371.

[28] H. Dong and K. Matyjaszewski, Macromolecules 41 (2008) 6868.

[29] D. Konkolewicz, A. J. D. Magenau, S. E. Averick, A. Simakova, H. He and K. Matyjaszewski, Macromolecules 45 (2012) 4461.

[30] D. R. D'hooge, D. Konkolewicz, M. Reyniers, G. B. Marin and K. Matyjaszewski, Macromolecular Theory and Simulations 21 (2012) 52.

[31] V. A. Williams, T. G. Ribelli, P. Chmielarz, S. Park and K. Matyjaszewski, Journal of the American Chemical Society 137 (2015) 1428.

[32] D. Konkolewicz, P. Krys, J. R. Góis, P. V. Mendonça, M. Zhong, Y. Wang, A. Gennaro, A. A. Isse, M. Fantin and K. Matyjaszewski, Macromolecules 47 (2014) 560.

[33] C. M. R. Abreu, A. C. Serra, A. V. Popov, K. Matyjaszewski, T. Guliashvili and J. F. J. Coelho, Polymer Chemistry 4 (2013) 5629.

[34] Q. Zhang, P. Wilson, Z. Li, R. McHale, J. Godfrey, A. Anastasaki, C. Waldron and D. M. Haddleton, Journal of the American Chemical Society 135 (2013) 7355.

[35] C. Waldron, A. Anastasaki, R. McHale, P. Wilson, Z. Li, T. Smith and D. M. Haddleton, Polym. Chem 5 (2014) 892.

[36] S. R. Samanta, R. Cai and V. Percec, Polymer Chemistry 6 (2015) 3259.

[37] S. R. Samanta, H. Sun, A. Anastasaki, D. M. Haddleton and V. Percec, Polym. Chem 5 (2014) 89.

[38] S. R. Samanta, R. Cai and V. Percec, Polym. Chem 5 (2014) 5479.

[39] C. Waldron, Q. Zhang, Z. Li, V. Nikolaou, G. Nurumbetov, J. Godfrey, R. McHale, G. Yilmaz, R. K. Randev, M. Girault, K. McEwan, D. M. Haddleton, M. Droesbeke, A. J.

Haddleton, P. Wilson, A. Simula, J. Collins, D. J. Lloyd, J. A. Burns, C. Summers, C. Houben, A. Anastasaki, M. Li, C. R. Becer, J. K. Kiviaho and N. Risangud, Polym. Chem 5 (2014) 57.

[40] L. Xue, Z. Lyu, X. Shi, Z. Tang, G. Chen and H. Chen, Macromolecular Chemistry and Physics 215 (2014) 1491.

[41] B. Lepoittevin, T. Elzein, D. Dragoe, A. Bejjani, F. Lemée, J. Levillain, P. Bazin, P. Roger and I. Dez, Carbohydrate polymers 205 (2019) 437.

[42] M. Bhattacharjee, N. B. Pramanik, N. K. Singha and D. J. Haloi, Polymer chemistry 11 (2020) 6718.

[43] J. Zhou, X. Zhou, Z. Dong, H. Yang, Z. Shi and R. Li, Applied Surface Science 279 (2013) 360.

[44] Sheriff Adewuyi Nurudeen O. Sanyaolu Saliu A. Amolegbe Abdulahi O. Sobola Olujinmi M. Folarin, Journal of Environmental Science 24 (2012) 1702.

[45] L. Sun, L. Zhang, C. Liang, Z. Yuan, Y. Zhang, W. Xu, J. Zhang and Y. Chen, Journal of Materials Chemistry 21 (2011) 5877.

[46] S. Yi, D. Lee, Y. Lee and E. Sin, Tetrahedron Letters 48 (2007) 6771.

[47] A. P. Alexandra, H. S. Mansur, F. P. Ramanery, L. C. Oliveira and P. P. Souza, Applied Catalysis B: Environmental 158-159 (2014) 269.

[48] P. Khoza and T. Nyokong, Journal of Molecular Catalysis. A, Chemical 399 (2015) 25.

[49] G. Huai-min and C. Xian-su, Polym. Adv. Technol. 15 (2004) 89.

[50] S. Adewuyi, I. Bisiriyu, C. Akinremi and S. Amolegbe, J Inorg Organomet Polym 27 (2017) 114.

[51] Adewuyi, S., Bisiriyu, I. O. and Akinremi, C. A., Ife Journal of Science 17 (2015) 749.

[52] B. Su and G. Feng, Polymer International (2010) 1058.

[53] T. DT and NT, An and NT Hoa, Chemical Sciences Journal 6 (2015) 95.

[54] Renata Czechowska-Biskup, Diana Jarosińska, Bożena Rokita, Piotr Ulański and Janusz M. Rosiak, Progress on Chemistry 12 (2012) 5.

[55] T. Wu and S. Zivanovic, Carbohydrate Polymers 73 (2008) 248.

[56] T. Y. Nikolaienko, L. A. Bulavin, D. M. Hovorun, Journal of Computational Chemistry 1050 (2014) 15.

[57] T. Y. Nikolaienko, and L. A. Bulavin, International Journal of Quantum Chemistry 119 (2019).

[58] I. O. Bisiriyu and R. Meijboom, Int. J. Biol. Macromol. 165 (2020) 2484.

[59] Garba Hussaini, Yakasai Jamila Bashir, Waziri Ibrahim, Bisiriyu Ibraheem O, Acta Scientific Pharmaceutical Sciences 4 (2020) 36.

[60] Sharma Ravi, Bisen D. P., Shukla Usha and Sharma B. G., Recent Research in Science and Technology 4 (2012) 77.